ICAS 2021 SHANG HAI
International Council of the Aeronautical Sciences
32nd Congress of the International Council of the Aeronautical Sciences
September 6-10, 2021
Pudong Shangri-La, Shanghai, China

LONGITUDINAL VORTEX FORMATION IN HYPRSONIC BOUNDARY LAYER ON BLUNTED DELTA WING AND ITS EFFECT ON FLOW CHARACTERISTICS

V.I. Shalaev[1], S.V. Alexandrov[1], A.V. Vaganov[2], M.A. Starodubtsev[2]
[1] Moscow Institute of Physics and Technology
[2]Central Aerohydrodynamic Institute

Abstract

Distinctive physical mechanisms of the longitudinal vortex formation, the high heat flux zone appearance and the early laminar-turbulent transition in hypersonic boundary layers on flat bodies with blunted leading edges are considered. To analyze these phenomena results of numerical simulations and experimental data for delta wings with blunted edges are used. Considered effects observed in many high-speed wind tunnel experiments but had not an explanation during a long time.

Keywords: *hypersonic flow, boundary layer, flat blunted bodies*

1. Introduction

A study of 3D hypersonic flows of a viscous thermo-conducting gas is actual problem of the today aerodynamics and has a significant interest for applications to developing a new generation of high-speed flying vehicles. Comprehensive investigations of these problems collide with difficulties due to limitations of experimental methods. Some progress reached using asymptotic methods and the boundary layer theory [1]. In these frameworks, basic controlling parameters for this flow class revealed effects of the viscous-inviscid interaction and disturbances propagation; the separation appearance in the laminar boundary layer were studied, self-similar solutions were constructed and heat exchange problems were considered.

In the same time, a set of phenomena observed in experiments still did not get an adequate explanation up to date. Zones of abnormal high heat fluxes and early laminar-turbulent transition on the windward surface of delta wings with blunted leading edges and on other similar configurations are appertained to such phenomena [2 – 10]. Effects of the Mach and Reynolds numbers, the bluntness radius and the angle of attack to these anomalies studied in details in wind tunnels. In all these works, surface phenomena were studied mainly using soot-oil or thermo-indicator coatings; plane shadow flow patterns did not allow clarifying a detailed spatial flow structure in order to relate it with observed effects. Thermoanemometer measurements of developing disturbances did not clarify also the problem essence [9].

The numerical modelling of the considered flow was conducted on the base of parabolized Navier-Stokes equations [11], Euler equations [10] and full Navier-Stokes equations [12, 13]. In the reference [7], the high heat flux spot observed on the wing leading edge near the nose and the S-shaped head shock wave were related with the flow reconstruction from the explosive type near the apex to the regime of the flow around the swept leading edge using the hypothesis about the hanging shock wave appearance due to the flow turn. However, the detailed visualization by the shadow method did not show the hanging shock wave in the transient region [8]. Solutions [11] revealed the presence of the intensive streamwise vortex near the wing symmetry plane, which was related with observed here extreme heat flux zone, but the mechanism of the heat exchange increasing was not clarified; the similar vortex was found also in solutions of Euler equations [10]. Over the middle span of the wing surface no flow structure peculiarities was found and a reason of the appearance here regions with high heat fluxes and early laminar-turbulent transition retained not clear.

This paper continues previous works [12-15], the detailed analysis of the flow structure around the delta wing is presented on the base of numerical solutions of Navier-Stokes equations. The

physical mechanism of the streamwise vortex formation over the middle wing part is directly related with the shape reconstruction of the bow shock wave near the nose. Effects of the vortex interaction with the boundary layer are analyzed. It allowed defining physical principals of the heat flux increasing and the early laminar-turbulent transition. Presented conclusions confirmed by old and new [16] experimental results.

2. Problem formulation

In the present work, hypersonic flows at Mach numbers M = 6 - 10.5, Reynolds numbers Re = (0.5 – 1.7)·10^6 around delta wings with the leading edge sweep angle $\chi = 75°$, the bluntness radius of cylindrical edges and the spherical nose R = 3 and 8 mm, angles of attack $\alpha = 0°$ and 10° are considered under experimental conditions [8 - 10]. It should be noted, all considered flow phenomena take place at different flow conditions and two angles of attack are selected as typical values. The mathematical wing model and used Cartesian coordinate system with the origin in the center of the nose bluntness are shown in the Fig. 1.

The wing surface is the flat plate with blunted leading edges and nose, it is supposed to be isothermal with the temperature factor about 0.4 in correspondence with wind tunnel experiments; no-slip conditions are used for the flow velocities. The flow is assumed to describe by full Navier-Stokes equations. All calculations were performed using the code ANSYS CFX (the license of DAFE MIPT).

The unstructured hexagonal grid constructed using the block method realized in the module HEXA is used. The grid model contained 7 blocks and 50 million nodes. Blocks with the minimal grid step been near the wing surface and its apex to resolve dynamical and temperature boundary layers and also large streamwise gradients of physical variables.

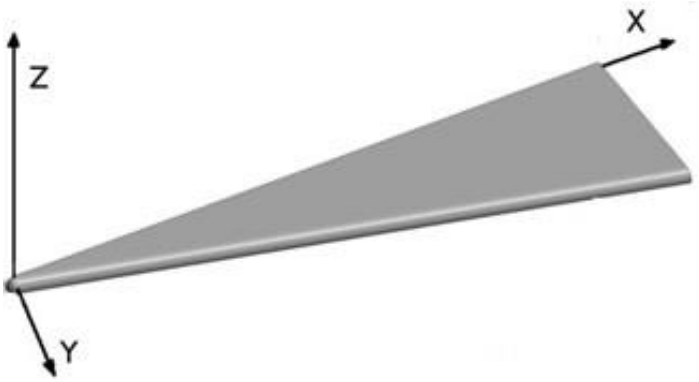

Figure 1 **–** The wing mathematical model

The grid contained 170 cells in the orthogonal to the surface direction; at least 10 cells were in the temperature boundary layer near the wing apex. About a quarter of all grid nodes were here and it ensures the well resolution. The maximum discrepancy for fluxes on the calculation region boundary was 10^{-6}, and inside the region it was 10^{-4}.

3. Flow structure near the leading edge and the local mechanism of heat flux increasing

In Figure 2, the qualitative picture of calculated heat flux distributions, $q = (\mu / \mathrm{Pr}) T_Z(X, Y, 0)$ (μ is viscosity, Pr is Prandtl number, T is temperature), on the leading edge and the main windward surface near the apex of the wing with the bluntness radius R = 8 mm at the angle of attack α = 10°, the Mach number M = 10.5 and the unit Reynolds number Re_1 = 4.1·10^6 m^{-1} are presented. In this figure, two zones of increased heat fluxes on the leading edge and the main wing surface remote from the apex about on ten bluntness radii (10R) are exuded clearly. Reasons of their formation are different and are considered below.

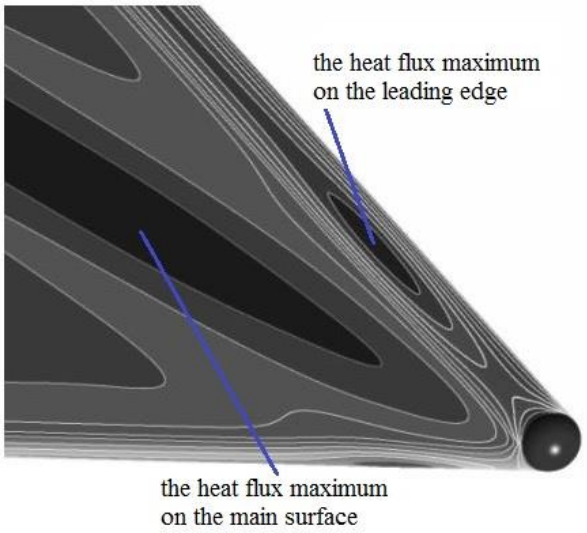

Figure 2 – Heat flux density distribution on the leading edge and the windward surface of the wing near the nose

In Figure 3, the comparison of experimental (symbols) and computed (lines) heat flux density distributions referenced to the stagnation point heat flux q_0 along the attachment line on the wing leading edge at α = 10°, R = 8 mm are presented for two flow conditions: M = 8.3 and $\mathrm{Re}_1 = 6.9 \cdot 10^6$ m^{-1} (the line 1) and M = 10.5, $\mathrm{Re}_1 = 4.1 \cdot 10^6$ m^{-1} (the line 2). The dotted line corresponds to the constant heat flux on the attachment line of the swept cylinder. It is seen, calculation results agree well with experimental data in the TsAGI wind tunnel T-117 [8]. The heat flux maximum is at the distance about 10R from the wing tip.

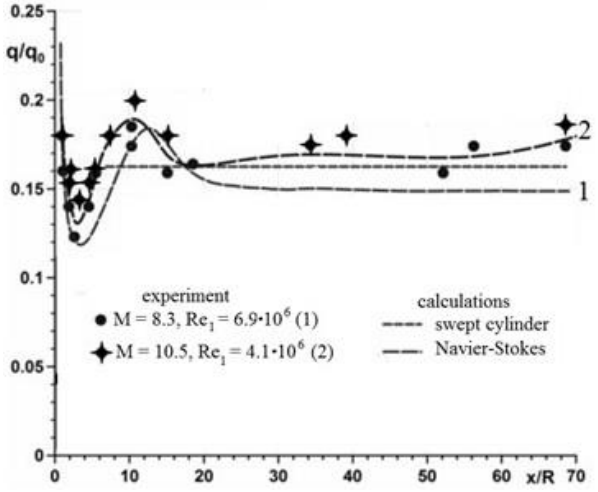

Figure 3 – Heat flux density distribution on the leading wing edge attachment line

In Fig. 4, the heat flux field on the windward wing surface and the flow static entropy field in the vicinity of the attachment line are presented for α = 10°, R = 8 mm, M = 8.3 and $\mathrm{Re}_1 = 6.9 \cdot 10^6$ m^{-1}. This figure illustrates the physical mechanism of the heat flux increasing on the leading edge. The outer boundary of the dark region corresponds to the bow shock wave having the S-shaped form due to the bending in the transient region between the explosive flow regime near the wing nose and the flow of the swept cylinder type far enough from the apex [6, 7, 11, 12]. At the end of the first zone before the bending, the shock wave tilt angle is smaller than at the swept leading edge regime. Here the flow after the shock wave has the smaller entropy and higher velocity directed to the leading edge. This flow presses to the surface the hot gas flowing from the near apex shock layer. Due to this effect the flow region between the wing leading edge surface and the shock wave

is narrowed that leads to reducing the velocity along the leading edge, to the higher heat flux and to increasing of the velocity in the transverse direction. The later effect is the one reason of the vortex formation over the middle wingspan.

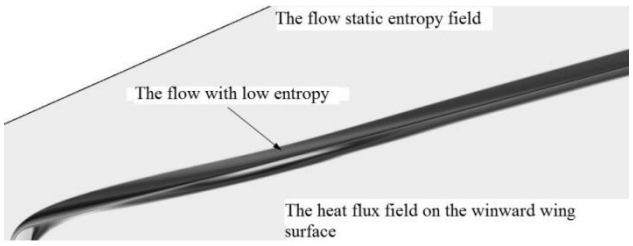

Figure 4 **–** The flow static entropy field (the upper part) and the heat flux field on the windward surface near the leading edge (the lower part)

From the comparison of Fig. 4 with results in Fig. 3, it is seen that the leading edge heat flux maximum (it is the center of the elongated light spot in Fig. 4) corresponds to about the narrowest flow part. The minimum heat flux corresponds to about the widest flow part located upstream in the explosive flow zone. Similar results were obtained for the smaller bluntness radius R = 3 mm and at α = 0° at different Mach and Reynolds numbers.

4. Distinctive properties and reasons of the heat flux and the laminar-turbulent transition over the main wing surface

Unusual properties of the heat exchange and the laminar-turbulent transition in the hypersonic boundary layer were found in wind tunnel experiments at the first on the surface of blunted half cones [2] and then on delta wings [3–10]. Specific heat flux distributions and limit streamlines on body surfaces are one of main results of hypersonic flow experimental investigations in wind tunnels, and they can be used for the numerical modeling verification.

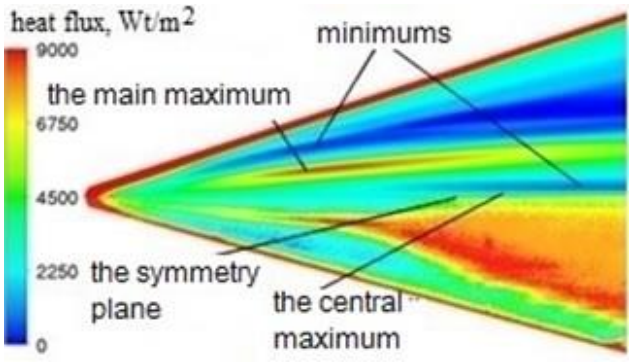

Figure 5 **–** Comparison of numerical (the upper part) and experimental (the lower part) specific heat flux distribution on the wing surface

In the upper part of Fig**.** 5, the calculated distribution of the specific heat flux on the wing surface with the length 0.57 m, R = 8 mm at α = 0°, the freestream Mach number M = 6, the unit Reynolds number $\mathrm{Re}_1 = 1.1556 \cdot 10^6\ \mathrm{m}^{-1}$, the total temperature T_0 = 750 K, the stagnation pressure P_0 = 20 atm are presented. The lower part of this figure corresponds to data obtained in the TsAGI shock wind tunnel UT-1M at about same conditions. Same results take place at other conditions on the downward wing surface at $\alpha > 0°$.

In the middle wing part, narrow streaks of the intensive heat exchange clearly identified as in calculations and experiments with the maximum specific heat flux q ≈ 8000-9000 Wt/m^2; this maximum depends mainly on Mach and Reynolds numbers and the bluntness radius. It should be noted in these streaks the heat flux increases to 3-4 times with respect to the background value that is compared with the laminar-turbulent transition effect and it can lead to unwanted consequences

on real flying vehicles. In experiments, these anomalies were known long enough [2] but reasons of their formation were not understand hitherto. As shown below, these anomalies relate with the streamwise vortex, the axes of which are over the streak and closer to the leading edge and follows to about the direction of its outer boundary.

Downstream, near the symmetry axis there is another higher heat exchange region with less values of the specific heat flux q ≤ 6750 Wt/m^2. It is shown below this anomaly is related with the elongated along the symmetry plane vortex; the location of this vortex with respect to the main vortex depends on flow parameters. The qualitative agreement of calculated and experimental distributions of the surface heat flux, at least up to the laminar-turbulent transition origin, allows hoping that considered flow structures are correctly reproduced by numerical modeling.

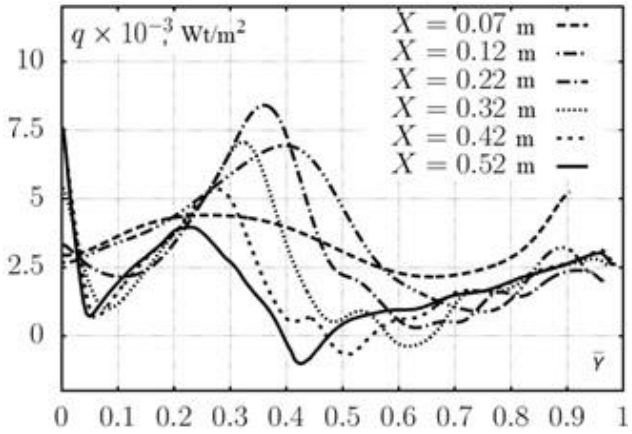

Figure 6 – Specific heat flux $q(\bar{Y})$ distributions on the wing surface

In Fig. 6 plots of the heat flux density distribution $q(\bar{Y})$ in different cross-sections of the wing X = 0.12, 0.22, 0.32, 0.42, 0.52 m are presented. The dimensionless transverse coordinate $\bar{Y} = Y / b$ is measured along abscissa axes, where $b(x)$ is the local half width of the wing. The maximum value of this function ($q_m \approx 8 \cdot 10^{-3}$ Wt/m^2) corresponds approximately to the point X_m = 0.2 m and $\bar{Y}_m$ = 0.4. This value exceed to 3-4 times the mean background value that compared with the growth of the heat flux in the laminar-turbulent transition. This circumstance does considered phenomenon very important for practical applications at large Mach numbers.

Results in the lower part of Fig. 5 show that in experiments the increased heat flux streak is expanded after reaching the maximum. This expansion is caused by the laminar-turbulent transition. It can notice the transition does not observed in regions located closer to the centerline and the leading edge, where known transition mechanisms work: Tollmin-Schlichting and cross-flow instability. The given in Fig. 5 transition observed in experiments on blunted wings and half-cones in hypersonic boundary layers only [2,3] and has a new type related exclusively with the evolving streamwise vortex: this type has a smaller transition Reynolds number. The mechanism of this phenomenon is considered below.

Considered above surface anomalies can be explained on the base of the analysis of the spatial flow structure, which is analyzed in details below for the case presented in Figs. 5 and 6. The general view of the flow structure in the cross-section X = 0.1 m after the formation in the apex vicinity of three vortexes with streamwise axis orientations is presented in Fig. 7. This cross-section locates over the beginning of the high heat-flux region on the wing surface, which is shown in the lower half of the picture. The blue streak in the cross-section corresponds to the shock layer formed near the wing apex and containing the high entropy gas; the boundary layer is below it (the light streak). It should be noted that in this section the gas temperature near the surface is essentially lower than in the shock layer. The cross flow has the domed structure, the region of boundary and

entropy layers expands in the direction to the symmetry plane that is related with the explosive character of the flow around the spherical nose in the hypersonic freestream. It is seen clear that in this cross-section three vortexes with approximately streamwise axes orientations have been formed already; the beginning of them formation locates in the wing apex vicinity.

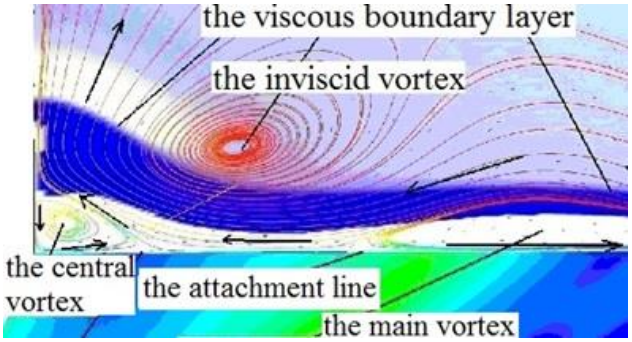

Figure 7 – The flow structure above the wing surface in the cross-section X = 0.1 m; α = 0°, M = 6, Re_1 = 1.1556·10^6 m^{-1}.

In the inviscid region above boundary and shock layers, the intensive clockwise rotating vortex has been formed; this vortex was found in solutions of Euler and parabolized Navier-Stokes equations [10, 11]. Its appearance is determined by the entropy layer thickening to the symmetry plane, i.e. by its domed shape and related with this effect the flow retardation in the direction to the symmetry plane.

Inside the boundary layer there are two counterclockwise rotating vortexes, which were found using Navier-Stokes equations only. The central vortex locates directly near the symmetry plane; its formation defined by the requirement of satisfying symmetry conditions inside the boundary layer, equations of which have the singularity in the delta wing symmetry plane [15]. The intensity of this vortex is small and the heat flux increasing under it is slight.

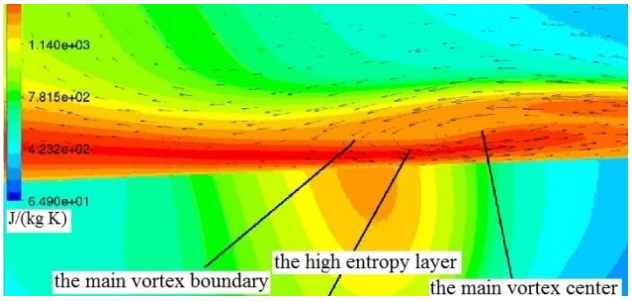

Figure 8 – Streamlines and the entropy distribution at the cross-section above the point of the heat flux maximum at the wing surface: X = 0.2 m, α = 0°, M = 6, Re_1 = 1.1556·10^6 m^{-1}

The second (main) vortex locates in the middle part of the wing span. The analysis of calculation results shown that this vortex is formed at the distance approximately 0.078 m (about 10 bluntness radii) from the wing apex under two opposite trends: 1) the growth of the cross velocity directed to the symmetry plane in the inviscid narrowing flow region between the shock wave and the leading edge; 2) the viscous flow of the opposite direction in the near-wall boundary-layer region defined by the cross pressure gradient induced by the viscous-inviscid interaction. Due to the boundary layer thickness growth and the diffusive absorption of the shock layer by the viscous flow these two regions with opposite velocities are converged, and at $X \geq 0.07$ m due to them interaction the rotated flow is formed. This vortex is in the boundary layer but its upper part is in the shock layer.

The flow structure can vary in dependence of the curvature radius, Mach and Reynolds numbers [8, 12]. The central vortex can be located upstream or downstream with respect to the main vortex or

don't arise. At large Mach numbers the middle flow region can contain two vortexes of opposite rotations but not the one vortex as in Fig. 7 [12].
In the upper part of Fig. 8, cross-flow streamlines and the entropy distribution in the section X = 0.2 m approximately corresponding to the specific surface heat flux maximum are presented. In the low part of Fig. 8 the heat flux distribution on the wing is shown.

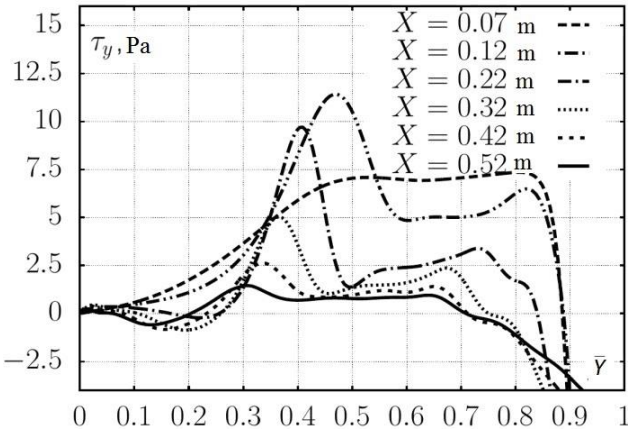

Figure 9 – Transverse skin friction $\tau_y(\bar{Y})$ distributions on the wing surface at α = 0° in sections X = 0.07, 0.12, 0.22, 0.32, 0.42, 0.52 m.

In Fig. 9 cross skin friction distributions $\tau_y(\bar{Y})$ in cross-sections X = 0.12, 0.22, 0.32, 0.42, 0.52 m are presented. It is followed from these data, specific heat flux distributions on Fig. 6 and the cross-flow attachment line, in which $\tau_y = 0$, formed by the vortex locates at the edge ($\bar{Y} \approx 0.22$) of the intensive heat exchange region, but the heat flux maximum corresponds to $\bar{Y} \approx 0.37$ in the section X = 0.2 m. The vortex center locates over the point $\bar{Y} \approx 0.43$ that corresponds to the maximum of the function $\tau_y(\bar{Y})$. It can see that in contrast to section of the increasing heat flux region beginning (X = 0.1 m, Fig. 6), in this section the gas with the highest entropy locates in the near-wall layer closest to the surface above the maximum heat flux point.

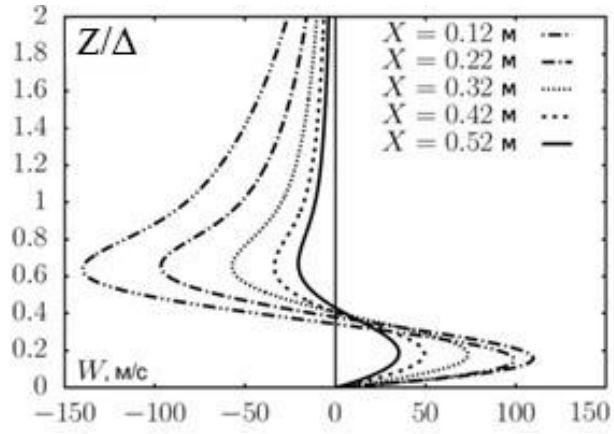

Figure 10 – Profiles of the cross-flow velocity along about the main vortex axis in sections X = 0.12, 0.22, 0.32, 0.42, 0.52 at α = 0°, M = 6, Re_1 = 1.1556·10^6 m^{-1}.

In Figs. 10 and 11 profiles of cross-flow ($W(\bar{Z})$, Fig. 10) and streamwise ($U(\bar{Z})$, Fig. 11) velocities along about the vortex axis are presented in cross-sections X = 0.12, 0.22, 0.32, 0.42, 0.52. In these plots, the dimensionless normal to the wing surface coordinate $\bar{Z} = Z/\Delta$ referenced to the local

boundary layer thickness Δ is measured along ordinate axes. These results demonstrate that the section of the maximum heat flux ($X \approx 0.2$ m) corresponds to the most vortex intensity (the cross-flow velocity maximum) and maximal transverse and streamwise shear stresses. Maximal cross-flow skin friction values on the wall at sections (Fig. 9) are achieved under the vortex axis. After the vortex formation in the section $X \approx 0{,}078$ m, its intensity growths downstream that indicates the cross-flow profiles (Fig. 10), and achieves to the maximum value in the section $X \approx 0.2$ m corresponding to the maximal surface heat flux. The comparison of transverse and streamwise velocity profiles also shows that the vortex region in two times thicker than the boundary layer if the edge of it is defined by streamwise velocity or temperature distributions.

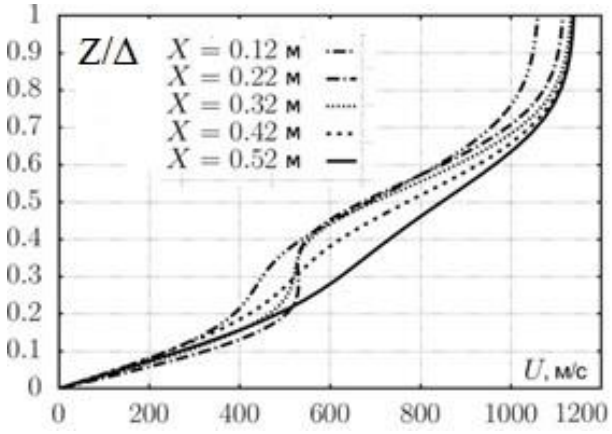

Figure 11 – Profiles of the logitudinal velocity along about the main vortex axis in sections X = 0.12, 0.22, 0.32, 0.42, 0.52 at α = 0°, M = 6, Re_1 = 1.1556·10^6 m^{-1}

In the section $X \approx 0.2$ m, the streamwise velocity profile becomes fully flat at the vortex axis (Fig. 11), and the cross-flow velocity near the wall achieves to the maximum $W \approx 110$ m/s, which about in 10 times less of the streamwise velocity. Downstream this section, the vortex weakens and the cross-flow velocity decreases. The streamwise velocity profile becomes more full but the inflectional point does not disappears that is very important circumstance for understanding the formed physical flow structure. It was noted above in the experiment (the lower half of Fig. 5) after the achievement of the maximum vortex intensity the laminar-turbulent transition is developed.

It should be noted the change of the heat flux larger than to three times, as its distributions in Fig. 6 show, can't be explained by the deceleration of the cross-flow. The enthalpy h and the temperature T in the near-wall boundary-layer region and also them normal derivatives at the wall can define by relations:

$$h = c_p T = H_0 - \frac{1}{2}\left(U^2 + W^2 + V^2\right); \quad h_Z\left(X,Y,Z\right) = H_{0Z}\left(X,Y,Z\right)$$

It is followed from the second formula, the heat flux directly relates with the total enthalpy derivative $H_{0Z}\left(X,Y,Z\right)$. On the wing surface flow velocities are zero and they don't influence to the heat flux. The normal velocity V in the boundary layer to an order less than the transverse velocity W, which in turn to ten times less than the streamwise velocity U. Therefore, variation of transverse and normal velocity can change the enthalpy on few percent only. It means that mainly the streamwise velocity defines the temperature distribution in the boundary layer.

Commonly the Reynolds analogy, which is relating linearly heat flux with the streamwise skin friction, is used for heat flux estimations. In the considered case, the largest streamwise velocity deformation and the growth of its derivative happen along the vortex axis (Fig. 11) and on the vortex periphery essentially weaken. Then, if the hypothesis about the similarity of streamwise skin friction and heat flux distributions would be true, the maximum surface heat flux would be observed

along the vortex axis. However, in calculations it is between locations of the axis and the cross-flow attachment line.

The detailed analysis of the spatial flow structure showed that in initial moments of the vortex formation the hottest gas is in the shock layer above the boundary layer, as it shown in Fig. 6. The vortex captures this hot gas and in the downward evolution process transfers it to the surface during the half turnover around the axis that is demonstrated in the figure 7. Inside the vortex, right from the attachment line the hot gas is pressed to the wall, where the higher heat flux region is formed. Left from the attachment line the vertical velocity is positive, the flow is directed to the outer boundary layer edge and the heat flux don't increase here. Therefore, the appearance of the extreme heat flux zone is defined by the convective vortex transfer to the wing surface of the hot gas with the increased full enthalpy from the shock layer located after the about direct shock wave before the nose. This conclusion is agreed also with the presented above relation for enthalpy derivatives, from which is followed that on the wall $T_Z \sim H_{0Z}$, i.e. the heat flux change is directly relates with increasing of the total local enthalpy.

Another result of the vortex-boundary layer interaction is the formation inside the later the velocity profile like to that of inside the twisted jet or the vortex in the cocurrent freestream. The velocity profile inside the boundary layer has the inflection point and even became flat near the vortex intensity maximum ($X \approx 0.2$ m). Such velocity profile is unstable with respect to Rayleigh mode, which is provoked the essentially earlier laminar-turbulent transition, than Tollmen-Schlichting waves [16]. On the other hand, the cross-flow velocity profile has the S-shaped form along the vortex axis that leads to the excitation of the cross-flow instability waves, which also lead to earlier transition [16]. The observed in experiments phenomenon (the lower part of Fig. 5) very reminds one of the laminar vortex breakdown scenario, defined by the development inside it unstable disturbances and the transition to the turbulence. What is transition mechanism at each concrete set of parameters – Rayleigh or cross-flow instability – it can be defined as a result of the considered flow hydrodynamic stability analysis that is out of these frameworks.

5. Conclusions

Presented results allow studying the hypersonic viscous flow structure over the windward surface of the delta wing with blunted leading edges or similar bodies. It permits explaining observed experimentally the high heat flux streak formation on the surface and the early laminar-turbulent transition in the boundary layer. Also it allows understanding physical principals leading to these phenomena. Numerical calculations were verified by comparison with experimental data.

It was found three types of streamwise vortexes formed over the wing near nose. The intensive vortex with the clockwise rotation forms in the inviscid flow region due to the cross-flow retardation because of its domed structure nears the symmetry plane. It was found also in solutions of Euler and parabolized Navier-Stokes equations. This vortex can't influence directly to the process of the heat exchange and laminar-turbulent transition.

Two other vortexes with the counterclockwise rotation form in the region including the hot shock layer and the boundary layer and they were obtained in solutions of full Navier-Stokes equations only. One vortex arises near the symmetry plane under the condition of the quick boundary layer retardation. The main vortex in the middle of the wing span forms due to the increasing of the cross-flow intensity in the transient region near the nose from explosive to swept flow regime and the viscous-inviscid interaction.

It was shown high heat flux streaks observed in experiments are defined by the convective transfer of the hot gas from the shock layer into the near-wall boundary-layer region. This is new mechanism of the shock and boundary layer interaction in spatial flows. In two-dimensional flows this interaction is defined by the diffusive absorption of the first by the second only. It is seen this new process leads to the appearance of the new physical effect.

The second effect of the vortex and boundary layer interaction leads to the inflection point formation

on the streamwise velocity profile and to the development of Rayleigh instability. The cross-flow velocity profile along the vortex axis has S-shaped form that leads to the excitation of the cross-flow instability. Both these phenomena lead to the earlier laminar-turbulent transition and to the vortex breaking that explains observed phenomena.

Copyright Statement

References

[1] V.Ya. Neyland, V.V. Bogolepov, G.N. Dudin, I.I. Lipatov. *Asymptotic theory of supersonic viscous gas flows*. Moscow, Fizmatlit, 2004.

[2] V.Ya. Borovoi, R.Z. Davlet-Kildeev M.V. Ryzhkova. On heat exchange peculiarities on the surface of some lifting bodies at large supersonic speeds. Izvestia RAN, MZhG, No. 1, 1968.

[3] I.A. Kondratiev, A.Ya. Yushin. On local heat flux increasing on the windward surface of a delta wing with blunted leading edges. *Aerothermodynamics of aerospace systems*, Report collection of TsAGI school-seminar “Mechanics of liquid and gas”, Zhukovsky, 1, pp. 167–175, 1990.

[4] O.I. Gubanova, B.A. Zemlyansky, A.B. Lesin, V.V. Lunev, A.N. Nikulin, A.V. Syusin. Abnormal heat exchange on the winward side of the delta wing with the blunted nose at hypersonic speeds. *Aerothermodynamics of aerospace systems*, Report collection of TsAGI school-seminar “Mechanics of liquid and gas”, Zhukovsky, 1, pp. 188–196, 1990.

[5] N.A. Kovaleva, N.P. Kolina, A.Ya. Yushin. Experimental investigation of heat flux and laminar-turbulent transition on half delta wing models with blunted leading edge in supersonic flow. Uchenye zapiski TsAGI, Vol. 24, No. 3, pp. 46–52, 1993.

[6] A.B. Lesin, V.V. Lunev. On peak heat fluxes on delta flat plate with blunted nose in hypersonic flow. Izvestia RAN, MZhG, No. 2, pp. 131–137, 1994.

[7] V.V. Lunev: *Flows of real gases with high speeds.* Moscow, Fizmatlit, 2007.

[8] V.N. Bragko, A.V. Vaganov, G.N. Dudin, N.A. Kovaleva, I.I. Lipatov, A.S. Skuratov. Experimental investigation of delta wing aerodynamic heating pecularities at high Mach numbers. Proceedings of MIPT, Vol. 1, No. 3, pp. 57–66, 2009.

[9] A.V. Vaganov, Yu.G. Yermolaev, A.D. Kosinov, N.V. Semenov, V.I. Shalaev. Experimental investigation of flow structure and transition in boundary layer on delta wing with blunted leading edges at Mach numbers 2, 2,5 and 4. Proceedings of MIPT, Vol. 5, Nj. 3(19), pp. 164-173, 2013.

[10] V.N. Bragko, A.V. Vaganov, V.E. Mosharov, V.N. Radchenko, S.V. Chernov: Calculated-experimental investigation of the flow structure over the windward surface of the delta blunted wing. Materials of XIV International school-seminar "Models and methods of aerodynamics", Evpatoria, pp. 28-29, 2011.

[11] V.I. Vlasov, A.B. Gorshkov, R.V. Kovalev, V.V. Lunev: Thin delta flat plat with blunted nose in viscous hypersonic flow. Izvestia RAN, MZhG, No. 4, pp. 134–145, 2009.

[12] V.N. Bragko, A.V. Vaganov, V.Ya. Neyland, M.A. Starodubtsev, V.I. Shalaev. Simulation of flow pecularities on delta wing windward side with blunted leading edges on the base of Navier-Stocks equation numerical solution. Proceedings of MIPT, Vol. 5, No. 2 (18), pp. 13-22, 2013.

[13] S.V. Aleksandrov, A.V. Vaganov, V.I. Shalaev. Physical Mechanisms of Longitudinal Vortexes Formation, Appearance of Zones with High Heat Fluxes and Early Transition in Hypersonic Flow over Delta Wing with Blunted Leading Edges. International Conference on the Methods of Aerophysical Research, Perm. AIP Conf. Proc. 1770, 2016. https://doi.org/ 10.1063/ 1.4963934.

[14] V.I. Shalaev. *Application of analytical methods in modern aeromechanics. Part 1. Boundary layer theory*. Moscow**,** MIPT, 2010**.**

[15] W.S. Saric, Y.L. Read, E.B. White. Stability and transition of three-dimensional boundary layers. Annual Review of Fluid Mechanics. Vol. 35, pp. 413-440, 2003.